IEEE Access
Multidisciplinary | Rapid Review | Open Access Journal

Received April 7, 2020, accepted April 20, 2020, date of publication April 24, 2020, date of current version May 11, 2020.

Digital Object Identifier 10.1109/ACCESS.2020.2990223

Two-Dimensional Multi-Ring Dielectric Lens Antenna to Radiate Fan-Shaped Multi-Beams With Optimum Adjacent-Beam Overlapping Crossover by Genetic Algorithm

HSI-TSENG CHOU[1], (Fellow, IEEE), YI-SHENG CHANG[2], HAO-JU HUANG[2,3], (Member, IEEE), ZHI-DA YAN[1], (Student Member, IEEE), TITIPONG LERTWIRIYAPRAPA[4], (Member, IEEE), AND DANAI TORRUNGRUENG[4], (Senior Member, IEEE)

[1]Graduate Institute of Communication Engineering, National Taiwan University, Taipei 10617, Taiwan
[2]Department of Electrical Engineering, Yuan Ze University, Taoyuan 32003, Taiwan
[3]National Chung-Shan Institute of Science and Technology, Taoyuan 32546, Taiwan
[4]Research Center of Innovation Digital and Electromagnetic Technology, Department of Teacher Training in Electrical Engineering, Faculty of Technical Education, King Mongkut's University of Technology North Bangkok, Bangkok 10800, Thailand

Corresponding author: Danai Torrungrueng (dtg@ieee.org)

This work was supported in part by the Ministry of Science and Technology, Taiwan, and in part by the King Mongkut's University of Technology North Bangkok under Contract KMUTNB-63-KNOW-026.

ABSTRACT A two-dimensional (2-D) discrete dielectric lens antenna is designed to radiate fan-shaped multi-beam patterns for gain stability in beam switching. The target is to minimize adjacent-beam overlapping transition regions and provide sufficient and similar gains for all field angles when the antenna is employed in a mobile device. This design starts with a conventional 2-D Luneburg lens antenna, and distorts its dielectric permittivity and the sizes of discrete dielectric rings to defocus the pencil beam patterns into shaped ones with a relatively flat pattern for uniform field distribution. The design is realistically implemented at 38 GHz with both simulation and measurement results shown to validate the concept. Successful validation of feasibility in beam synthesis is achieved. Fabrication discrepancy to result in slight radiation degradation is also discussed.

INDEX TERMS Genetic algorithm, Luneburg lens antenna, multi-beam radiation, pattern synthesis.

I. INTRODUCTION

User equipment (UE) or customer-premises equipment (CPE) antennas in mobile or fixed network communications [1] require high gains in radiation to compensate electromagnetic (EM) wave propagation loss in air [2] which is severe at millimeter wave (mmW) frequencies. Conventional implementation of a phased array of antennas to produce electronically steering beams is very cumbersome as it involves numerous costly RF devices. Their realization on dielectric substrates also faces severe challenge of power loss in the lossy substrates when beamforming networks (BFNs) are implemented by microstrip lines. Instead, multi-beam antennas are among the potential solutions to provide high directional beams of easy switch at a much lower cost.

Due to the dynamic changing of position and orientation in UE and CPE usage scenario, multi-beam radiations with a fan-shape pattern [3], [4] (i.e., vertically broad and horizontally narrow to perform horizontal beam switching) is very attractive because a single one-dimensional (1-D) beam scan, instead of applying sophisticated two-dimensional (2-D) ones, is sufficient to provide the required gain. Moreover, a flat-top pattern is most desired along the beam scan dimension to provide seamless connection links with relatively uniform gain performance. This importance has been well-documented in literatures for various antenna designs [5]–[11]. Potential antenna candidates include a 1-D phased array of antennas with proper BFNs and 2-D Luneburg lens antennas [12]–[14]. More advantageous than a phased array

The associate editor coordinating the review of this manuscript and approving it for publication was Chow-Yen-Desmond Sim.

This work is licensed under a Creative Commons Attribution 4.0 License. For more information, see https://creativecommons.org/licenses/by/4.0/

of antennas, which suffer from limited beam scan range due to high wide angle scan loss, a 2-D Luneburg lens is rotationally symmetric to provide equal gains for all beams with broad frequency bandwidth in terms of reflection coefficients and radiation characteristics when the feed has broad operational bandwidth.

It is noted that the conventional implementation of multi- or steering beams gives rise to severe drawbacks for producing discrete beams when digital phase shifters and multi-feeds are employed in phased array antennas and Luneburg lens antennas, respectively. For the case of Luneburg lens antennas, the best gain at the crossover point of two adjacent beams is smaller than -6 dB below the beam peak due to limited space for feeds as shown in Fig. 1(a) when they are excited by classic waveguides of fundamental modes. Insufficient gains appear in the transition regions to cause power instability by frequent handovers (i.e., the ping-pong effect) [15], where call drops may also happen. It is noted that even though a smaller gain-drop at the crossover point of approximately -3 dB was claimed in [16] by using transmission line excitations for more crowded feeding ports, where numerical simulation results were shown, the inter-port isolation has been significantly degraded so that it is worse than -15 dB, and the back-lobes are significantly high due to the radiation from the transmission line exciting port. Moreover, experimental validation has not been shown. This increase of excitation ports will make the system implementation more sophisticated.

This paper presents a 2-D lens antenna design for the first time to radiate relatively uniform patterns as illustrated in Fig. 1(b) to reduce the adjacent beam transition region for beam stability at mmW frequencies, also applicable to CPE of front-haul networks. It is noted that front-haul networks are currently viewed as the most important application in the first stage of commercial 5G (the fifth generation) mobile communication system at mmW frequencies. The fan-shaped patterns with relatively flat-top patterns provide a very simple connecting mechanism between the base station and CPE antennas by performing a 1-D beam scan. The flat structure of 2-D Luneburg lens can be implemented inside a PCB, which can be integrated with the multi-layered substrate based hardware system for compactness.

The design uses the genetic algorithm (GA) as a tool, and starts with an initial design by a discrete 2-D Luneburg lens [17]–[19] to assure the property of directional beams. Its permittivity and sizes of discrete dielectric rings are then optimized by the GA [20]. In contrast to previous works of three-dimensional (3-D) Luneburg lens optimization, which either minimize the estimation error of permittivity [21] in a least squares error (LSE) sense, or enhance the gain and reduce sidelobe levels (SLLs) [22], [23], we focus on the 2-D main beam synthesis for CPE applications. The major target is to simultaneously reduce the inter-beam transition area [24], and minimize gain variation, i.e., creating a more uniform field. This optimization is more challenging than

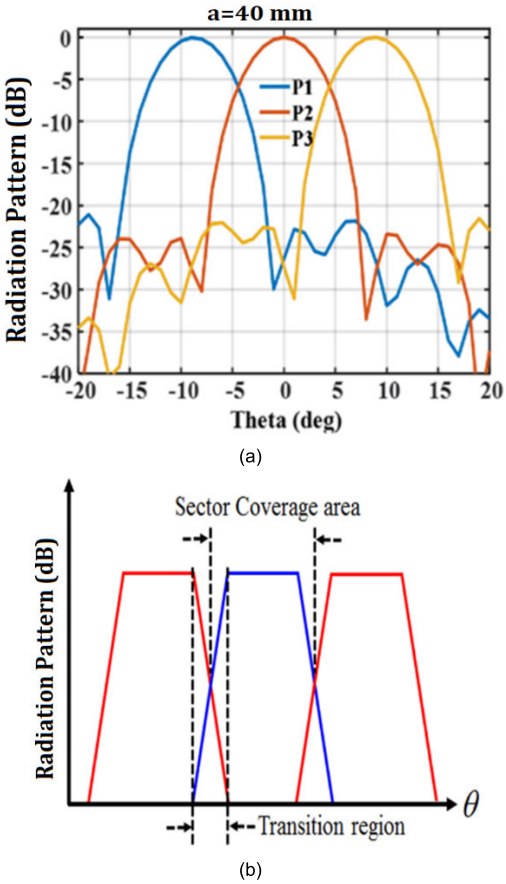

FIGURE 1. Beam overlapping of a conventional Luneburg lens antenna, and the desired patterns of multi-beams with small transition regions. In (a), the radius is 40 mm at 38 GHz, which will be explained in Section II.A. (a) Beam overlapping; (b) Desired patterns.

the uniform permittivity lens optimization on its external surface profile [20], [25] because of the limited parameters available for optimization of retaining symmetric multi-ring structures. After the optimization, the radiation patterns are compared to that of conventional Luneburg lens antennas at 38 GHz. Radiation measurements on an antenna prototype are also presented to validate the design feasibility. Numerical results show that the gain-drop at the crossover point is less than 1 dB in addition to the flat-top main beam pattern for stable coverage, exhibiting much better behavior than that in [16]. The low crossover point gain drop is also validated by measurement results.

The rest of the paper is organized in the following format. Section 2 presents the basic radiation behavior of 1-D multi-beams by Luneburg lens, and shows the pattern synthesis for better communication links. Section 3 presents the basic implementation of GA to synthesize the radiation patterns of a 2-D dielectric lens. Parametric studies of GA optimization are also shown. A realistic design is shown in Section 4 for validation of this proposed work of a multi-beam lens antenna design. Finally, a short discussion is presented in Section 5 as a conclusion.

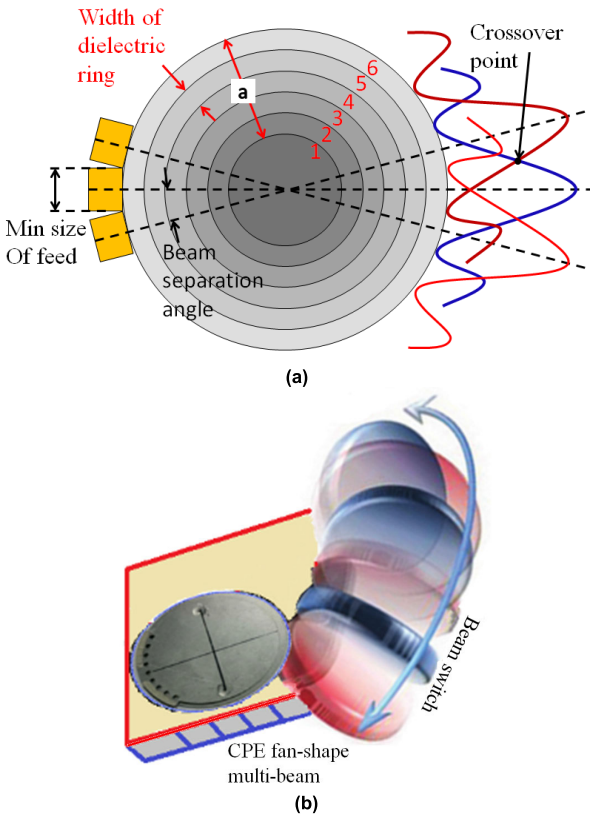

FIGURE 2. Illustration of discretized Luneburg lens and its architecture as a multi-beam antenna, where the feeds and radiation beams are also illustrated. (a) shows the concept while (b) shows the application for a CPE antenna. (a) Concept; (b) CPE application.

II. DESIGN CONCEPT AND OPTIMIZATION

A. ARCHITECTURE OF LUNEBURG LENS AND PROBLEM STATEMENT

A 3-D Luneburg lens is an inhomogeneous dielectric sphere with varying relative permittivity governed by [12]–[14], [17]–[19]

$$\varepsilon_r(r) = 2 - (r/a)^2, \tag{1}$$

where r is the radial distance and a is the sphere radius. In practice, the 2-D Luneburg lens is a dielectric slab sandwiched by a pair of parallel metal plates, where the dielectric slab is formed by a finite number of uniform, concentric dielectric rings of various widths, as shown in Fig. 2 (a), where its potential application as a CPE antenna is also shown in Fig. 2(b). The widths and relative permittivity values of the dielectric slabs are determined by optimization schemes according to different mechanisms as mentioned in [20]–[25].

Based on realistic feed antennas at a separation distance of larger than a half-wavelength, the crossover point of two adjacent beams is more than -6 dB below the beam peaks as shown by the HFSS simulated results in Fig. 1 (a), where $a = 40$ mm, and 10 rings (including an air ring) are used. Their widths and relative permittivity values of the dielectric slabs are determined by the optimization scheme in [4] and [21]. It is fed by rectangular waveguides ($0.7 \times 0.35\lambda^2$ in aperture size, where λ is the wavelength of free space) placed tightly to each other.

Numerical experiments show that the larger 6 dB gain drops in the transition regions in Fig. 1(b) are similar for any Luneburg lens regardless of its size of lens except for slight inwardly shifted beam directions due to the smaller angular span occupied by the feeds' physical size when a larger lens is considered. The gain drops are even worse when the two adjacent feeds are further separated to increase the isolation between them. This problem results naturally from the radiation phenomenon of a pencil beam shape, and may cause the pin-pong effect due to insufficient gain. This is most undesired because the possibility of dynamic moving will worsen the stability of connection to the base station antenna.

In this paper, we propose to synthesize a shaped beam to alter the beam overlapping by pencil beams as shown in Fig. 1(a), where the desired one is shown in Fig. 1 (b). In this case, the beam overlapping region is reduced to avoid hand-overs while the beam connection has a high stability due to its uniform field distributions in the main beam regions. This shaped beam pattern synthesis is described below.

B. DESCRIPTION OF RADIATION BEAM PATTERN OPTIMIZATION

The beam shape in Fig. 1(b) is synthesized in the lens design with a cost function first defined by

$$F = \sum_{m-1}^{M} f_m \left| G_m - G_m^d \right|^2, \tag{2}$$

where G_m^d and $G_m$are the desired and computed gains at the M sampled field points. In (2), f_m is used to balance the field weightings of main beam to the sidelobes in the transition regions, where $f_m = 1$ is assumed for simplification because we focus on the main beam pattern. The shaped beam is particularly performed to optimize the main beams for better field distribution with minimum overlapping.

The parameters of the lens structure used in the optimization include the overall size, the widths of dielectric rings and their permittivity values. In particular, the relative permittivity is relaxed to be larger than 2 while retaining its sequential decrease from the center to its boundary for air ring matching. Only a single beam is considered for the circular symmetry of the lens, where HFSS is employed to compute the radiation. In GA [20], [26] optimization, each optimization parameter is represented by a *3*-bit variable. In order to assure a gradual decrease of relative permittivity, one first selects reference values by performing the algorithm in [4], [21] to minimize the estimation error with respect to (1) as indicated by the black stepped lines in Fig. 3. Afterward, a variation range is selected for the theoretical values between the two boundaries of a selected dielectric ring inside the two red dashed lines in Fig. 3.

To relax the variation of relative permittivity, (1) is modified by

$$\varepsilon_r(r) = 2\alpha - 2(2\alpha - 1)(r/a)^2, \tag{3}$$

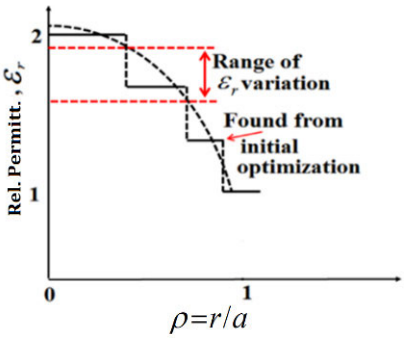

FIGURE 3. Illustration of the relative permittivity variation range for optimization, which is set up by using the estimation in (1) as initial values.

where α is the modification factor, which is slightly larger than 1. The relative permittivity of the most outer ring reduces to 1 for the air while that at the central ring may be larger than 2. This range of dielectric constant may allow the lens to retain the basic property of a directional beam as provided by the 2-D Luneburg lens.

III. PARAMETRIC STUDY IN GA 2-D LENS ANTENNA SYNTHESIS

One first examines the effectiveness of optimization for a 2-D Luneburg lens by the GA with a thickness of 2.84 mm which is the thickness of the feeding rectangular waveguide. This lens has an initial radius of 27.5 mm at 38 GHz, and is sandwiched by a pair of circular metal parallel-plates to form a cavity. The target gains are 11dBi for the flat part in Fig. 1 (b), where the fields in this flat region within a beamwidth of 16 degrees are sampled to compute the cost function in (2). As pointed out in Section 1, the desired radiation has fan-shaped patterns, i.e. vertically broad and horizontally narrow, to perform a 1-D scan. In particular, a uniform distribution of main beams, as illustrated in Fig. 1 (b), is desired in order to retain gain stability when the multi-beams are discretely switched. It may potentially provide a seamless transition when the beam is switched from one to another.

In the synthesis stage of examining the effectiveness of the GA application, the feeds are rectangular waveguides with a cross-section of 5.68 $\times$ 2.84 mm^2 to excite TE_{01} modes and investigate the radiation characteristics. A compact embedded probe excitation will be implemented for the later antenna prototype design as well as for the numerical and experimental validation.

A. PARAMETERS EMPLOYED IN GA OPTIMIZATION

The parameters in the GA synthesis are first described in this section. In these examinations, either the thickness of dielectric rings, dielectric constants or both is considered in the synthesis to exhibit their characteristics. For all cases, 8 populations and 4 generations are employed, where each population consists of 6 chromosomes of 3 parameters of thicknesses and 3 parameters of dielectric constants for the dielectric shells. Each chromosome is represented by 3 bits of binary expression. In the case of synthesis, the average CPU time is roughly 16.5 minutes on an i7-7820X processor. In addition, they all start with same values for their geometrical parameters and relative permittivity values as shown in Table 1. This set of initial values is obtained by using the optimized selection of discretized parameters of the Luneburg lens in (1) as suggested in [4], where four rings are considered including three dielectric rings and an air ring for cost consideration.

TABLE 1. Initial values of geometrical parameters and relative permittivity.

Shell Index	1	2	3	4
Thickness (mm)	15.88	6.57	5.05	2.2
Relative permittivity	1.76	1.48	1.23	1 (air)

The four cases examined consider the four combinations of parametric variables by the dielectric constants and the ring thicknesses. In particular, the first case of synthesis considers the dielectric constants of each rings as the optimization variables, where the variation of dielectric constant in (1) is employed to discretize the ranges for optimization of each ring in Fig. 3. In this case, the thicknesses of each ring remains fixed, as in Table 1. Thus the maximum dielectric constant in Fig. 3 is 2. On the other hand, the second case also considers the dielectric constants of each ring as optimization variables under similar conditions except now (3) is employed to specify the ranges of dielectric constants for each ring to optimize their dielectric constants. The other two cases of optimization, which are referred to cases 3 and 4 in Table 2, add the thicknesses of each ring, D_n, as the optimization variations to the first two cases.

In the GA implementation of dielectric ring thicknesses as optimization variables, one considers the ratios of thicknesses to a fixed size of lens. It is performed by using 3 digits to discretize the range of variation into 8 steps ($1 \sim 8^{\text{th}}$ step). Let each ring's thickness be represented by S_n in the discretized representation, then the thickness of the n^{th} is given by

$$D_n = \frac{S_n}{\sum_{n-1}^{N} S_n} a, \tag{4}$$

where a is the selected radius of the lens including the air ring. Once the thicknesses are determined, the ranges of each ring to determine their dielectric constants in Fig. 3 are specified. Similarly, three digits are employed to discretize each of the ranges and represent the variations of dielectric constants in these ranges.

B. EFFECTIVE OF 2-D LUNEBERG LENS OPTIMIZATION

Due to the rotationally symmetric configuration, a single beam is considered for simplification, where the co-polarized (Co-pol) patterns of this initial architecture on the E- and H-planes are shown by the black lines in Fig. 4(a) and (b), respectively, which serve as reference

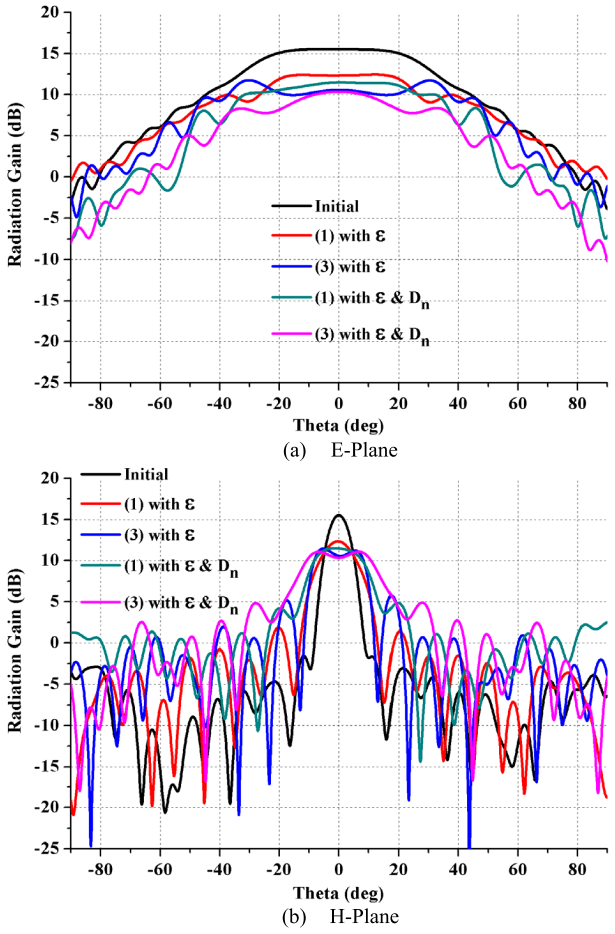

FIGURE 4. Radiation patterns of optimized Luneburg lens, where different optimization variables are used in the synthesis.

patterns for comparison. The gain is roughly 15.5 dBi with a -3 dB beamwidth of 7.9 degrees along the multibeam dimension. The relative SLL is roughly -17 dB below the main beam peak. As described in Section II, the target beamwidth of the desired flat patterns in Fig 3 is 16 degrees. The roll-off rate on both sides of main beam curve depends on the size of the resulting lens.

The resulting values of variables by GA optimization for the four cases are summarized in Table 2. It is observed that cases 1 and 3 result in a converged relative permittivity of nearly 1.99 for the central dielectric disks. On the other hand, cases 2 and 4 result in an optimized relative permittivity of 2.38 and 2.47, respectively, which are larger than 2 as desired in the original Luneburg lens design in (3). On the other hand, the third rings of cases 1 and 3 are close to free space, where the relative permittivity values are roughly 1.05. In addition, the thicknesses of the first and third shells are almost equal after synthesis.

The resulted radiation patterns on the two principal planes corresponding to the four cases of Table 2 are shown in Fig. 4(a) and (b), respectively by different color lines in comparison to the patterns of the initial design in Table 1. In all cases, the E-plane patterns are relatively broad due to

TABLE 2. Comparison of optimized parameters of Luneburg lens antenna.

Case	Optimization approach		Shell Index			
			1	2	3	4 (air)
1	(1)	ε_r	1.99	1.38	1.05	1
2	(3)	ε_r	2.38	1.64	1.44	1
3	(1) + D_n	ε_r	1.99	1.75	1.08	1
		D_n (mm)	8.59	10.32	8.59	
4	(3) + D_n	ε_r	2.47	2.13	1.13	1
		D_n (mm)	9.82	7.86	9.82	

the thin thickness of the 2-D lens. The -3 dB beamwidth is roughly 60 degrees to provide a wide coverage. The gain drops by roughly 3-5 dB caused by the H-plane pattern optimization for the flatness of the central main beam area. The H-plane patterns, which are used to form the multi-beams, have larger variations because of the optimization to achieve flat patterns in Fig. 3.

It is first observed that the case 1 of using (1) with a maximum of 2 at the center of the Luneburg lens only results in a broader pattern without changing the pencil beam shape, which does not fulfill the target pattern in Fig. 3. On the other hand, the remaining three cases may result in relatively flat main beam patterns. In comparison, the main beam shape in the second case, by using (3) to set the variables of optimization, descends very rapidly near the boundary of flat main beam region, where the -1 dB beamwidth is 15.5 degrees while the -3 dB beamwidth is 18.7 degrees. In this case, α in (3) is set to be 1.5 to make a relative permittivity of 2.38 for the central dielectric disk. Also the fourth case of using both (3) and the thicknesses of dielectric shells as the optimization variables results in the largest beamwidth with a smaller slope of descent for its main beam shape near the boundary, which may result in a larger overlapping area between two adjacent beams. All these three cases result in similar SLLs, which are roughly -6 dB below the main beam peak. This side lobe discrepancy can be improved by using H-plane rectangular horns as the feed to create a tapered illumination.

IV. DESIGN IMPLEMENTATION OF VALIDATION

A. A REALISTIC DESIGN FOR EXPERIMENTAL VALIDATION

The antenna is designed and prototyped for validation of feasibility at a 38 GHz band, where the achieved geometrical parameters and relative permittivity are summarized in Table 3. The radius of the lens is 50 mm with a thickness of 2 mm, which is larger than these in Table 2 in order to further control the SLLs by a larger aperture. The paired circular metal parallel-plates sandwiching the lens has a radius

TABLE 3. Synthesized values of geometrical parameters and relative permittivity.

Ring Index	1	2	3	4
Width (mm)	28.87	11.95	9.18	3
Relative permittivity	1.82	1.73	1.28	1 (air)
Teflon thickness (mm)	1.50	1.30	0.50	0

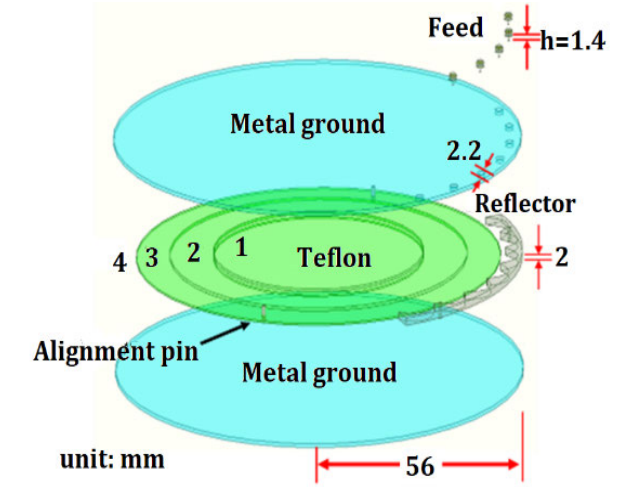

(a) Architecture

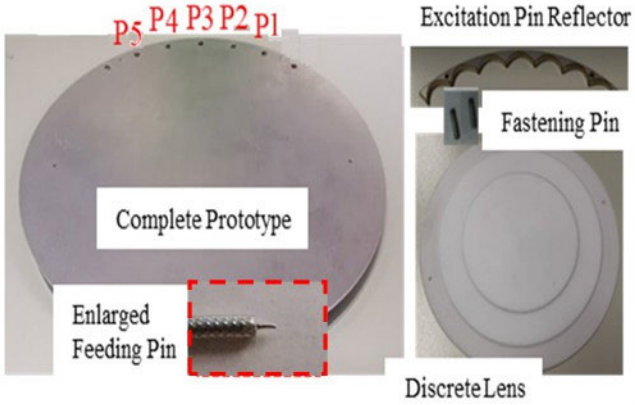

(b) Prototype

FIGURE 5. Numerical model and prototype of the 2-D multi-beam lens.

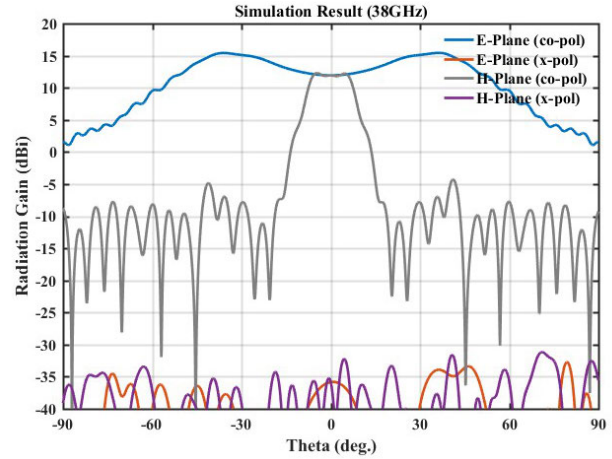

(a) Simulation

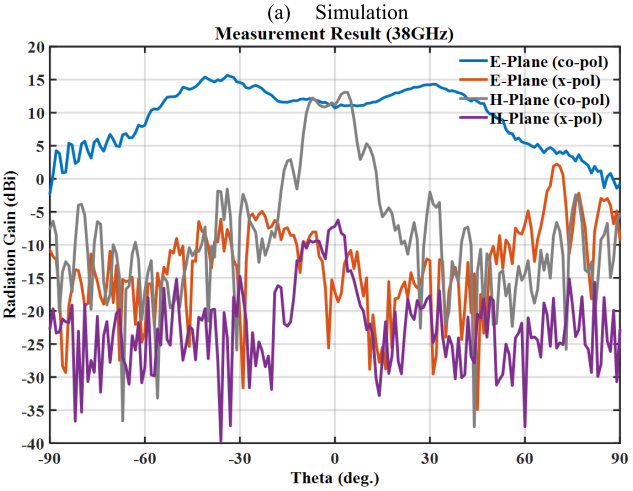

(b) Measurement

FIGURE 6. Radiation patterns of a 2-D Luneburg lens antenna.

of 56 mm, slightly larger than the lens to increase isolation to the nearby RF devices for future applications. In this design, 4 dielectric rings (including an outer air ring) are employed to form the lens. The incident wave illuminating the lens is excited by a probe pin backed by a metal parabolic reflector at 38 GHz as shown by the numerical model and prototype in Fig. 5. The prototype is hand-assembled after every component is fabricated.

For the prototype implementation, the slab of each dielectric ring is equivalently resembled using two stacked layers of Teflon and air [4] whose thickness ratio is selected to make the average relative permittivity equal to the computed ones in Table 1. In this case, five beams are implemented, where the feeding structures are illustrated in Fig. 5. Detailed structures are referred to [4] for brevity.

B. RADIATION CHARACTERISTICS

The simulated and measured radiation patterns are shown in Fig. 6(a) and (b), respectively, where relatively uniform fan-shape patterns are seen in the simulation results as expected. The good agreement between simulation and measurement is achieved with some slight discrepancy in the measurement results due to prototyping discrepancy. The gain variations are relatively uniform on the main beams, where the gain is larger than the targeted value of 11 dBi in the synthesis. The relative cross-polarization level (XPL) is less than -40 dB from the numerical simulations in Fig. 6 (a), which is slightly higher in measurements due to the difficulty of accurate alignment for hand-assembly since the parallel-plate antenna structure is well-known to have good polarization characteristics.

The simulated and measured reflection coefficients are shown in Fig. 7 (a) and (b) respectively, where both exhibit very broad frequency bandwidths. The simulation reflection coefficient level is below -15 dB for most frequencies while

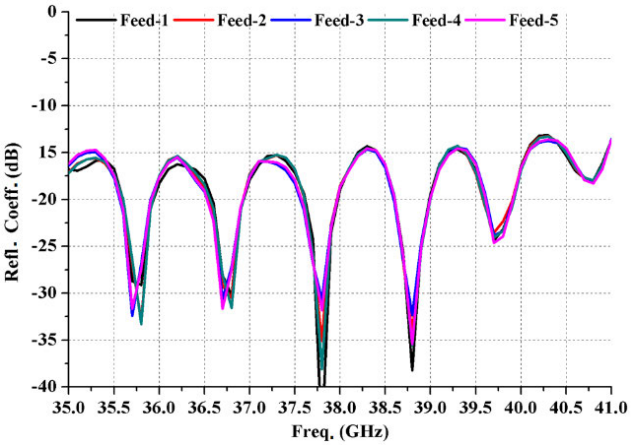

(a) Simulation

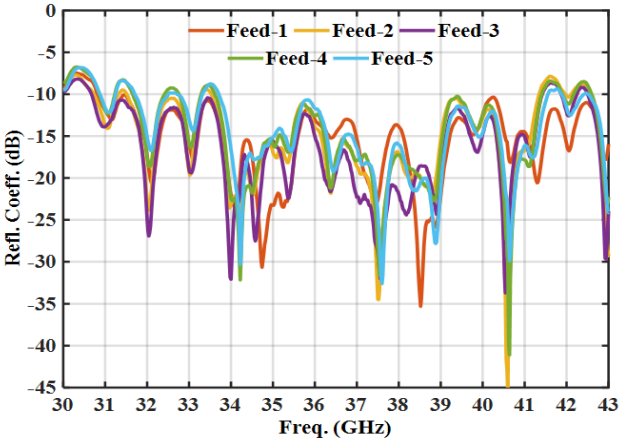

(b) Measurement

FIGURE 7. Simulated and measured reflection coefficients.

it is higher in the measurement results due to the fabrication discrepancy and K-type connector implementation. However, the agreement with the simulation results is in general very good, where the -10 dB bandwidth is more than 7.5 GHz in measurement results.

C. CHARACTERISTIC DISCUSSIONS

One first considers the multi-beam distribution in Fig. 8 (a) and (b) for the simulation and measurement results respectively, where good agreement has been achieved. The asymmetric measured patterns of wide-angle beams on both sides are attributed to the discrepancy of hand-assembly and alignment for wide angle patterns in a 2-D far-field measurement system. In this case, the overlapped patterns along the H-plane are relatively uniform, almost 12 dBi in gain in the region covered by these beams. The crossover points are roughly 0.5 dB below the flat top. The roll-off rate of the main beam boundary is much higher than that in Fig. 1 (a), indicating a much smaller transition region. Similar behaviour is also observed on the measurement result even though the first sidelobes are much larger than that of the simulation. Finally, the isolation of beam ports is investigated by considering that between ports 4 and 5, as shown in Fig. 9.

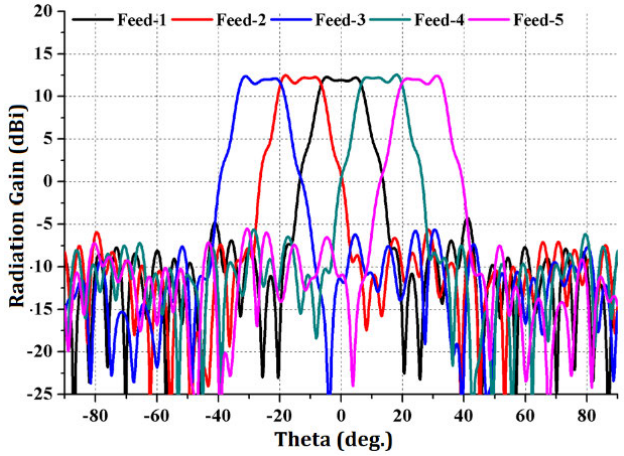

(a) Simulation

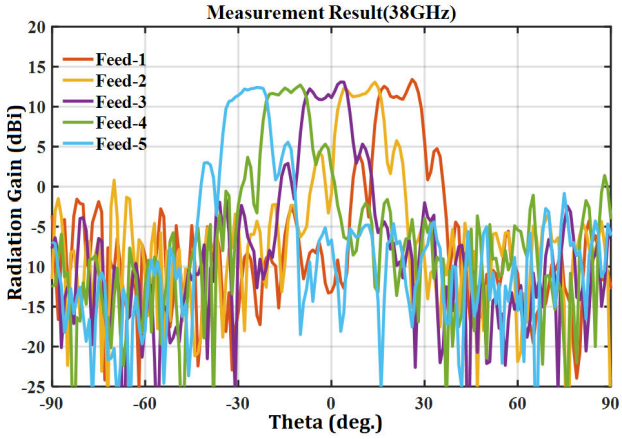

(b) Measurement

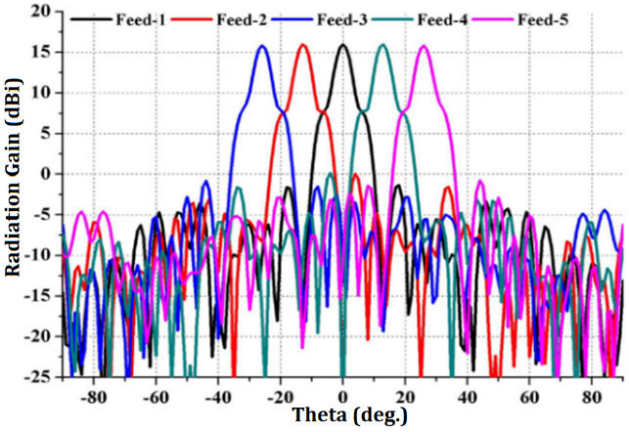

(c) Simulated multi-beam from the lens without optimization

FIGURE 8. Multi-beam overlapping of the 2-D lens antenna. (c) is the simulated results of a Luneburg lens under the same condition of size and feeding.

It is observed that the isolation is better than -20 dB in both simulation and measurement. The other ports have similar behaviors, which are omitted for simplification.

To further examine the effectiveness of fan-shaped beams, the multi-beam radiations of a Luneburg lens without optimization under the same conditions of size and feeds are shown by the simulation results in Fig. 8 (c). It is seen that

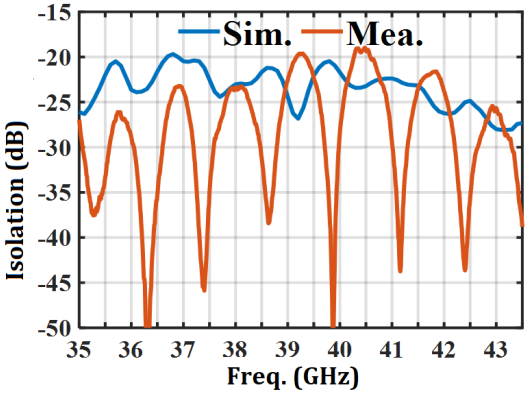

FIGURE 9. Simulated and measured Isolations between ports 4 and 5. The other ports have similar behavior.

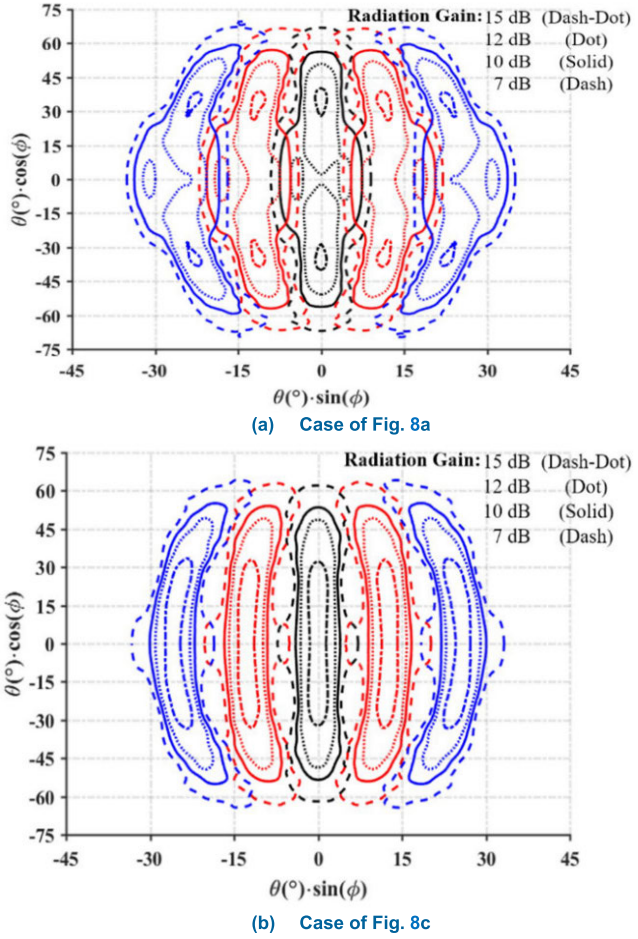

FIGURE 10. Simulated contoured patterns to compare the coverage between the cases of Fig. 8(a) and (c) with and without synthesis for shaped patterns, respectively.

the gains are roughly 15.5 dBi, which is 3.5 dB larger than the designed one. However, the crossover point is at 8 dB below the beam peak. Thus, in the transition region near the crossover point, the received EM power by the UE will be 8 dB smaller. On the other hand, in the transmitting mode with power control, the EM power in the beam peak direction is 8 dB larger, and causes severe interferences to the other UEs.

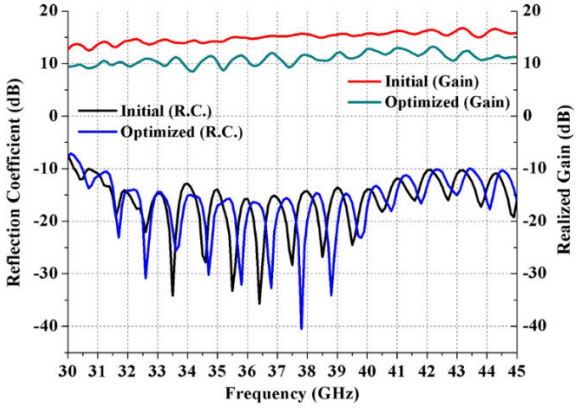

FIGURE 11. Examination of frequency stability for the 2-D Luneburg lens antenna with and without main beam synthesis, where the gain and reflection coefficients are compared.

The simulated contoured patterns in the cases of Fig. 8 (a) and (c) are shown in Fig. 10 (a) and (b), respectively. If one considers a 10 dBi gain as the threshold of coverage area. It can be seen that Fig. 10 (a) shows a coverage with much better uniform field distribution inside the coverage area, indicating a better fan-shape pattern along beam switching, resulting in a smooth beam transition for CPE connections.

Finally, the frequency stability, by comparing the cases with and without the GA synthesis, is shown in Fig. 11, where simulated gains and reflection coefficients (R.C.) are shown. It is observed that the reflection coefficients remain relatively stable when the lens is synthesized. On the other hand, the synthesized gains exhibit higher fluctuations of roughly 1 dB.

V. CONCLUSION

In this paper, we present a 2-D lens antenna design for fan-shaped multi-beam radiations with relatively uniform patterns to minimize the beam overlapping transition regions, where a GA was employed to synthesize the discretized dielectric rings in the widths of dielectric rings and their permittivity. Distinguished radiation characteristics have been shown in both the simulation and measurement results, which provide the advantage of increasing better gain in the transition region of adjacent beams for the stable power control. Currently, only the main beams are employed in the pattern synthesis, and may result in higher sidelobes. Our experimental experience indicates that manufacturing discrepancies may result in significant radiation distortion leading to a loss of uniform shape and a reduction in the conventional pencil beam when the operational frequency is far away from the design central frequency. However, the gain and reflection coefficients have relatively high stability with respect to frequency change. This phenomenon is caused by the limited few available parameters in the GA synthesis.

REFERENCES

[1] M. Agiwal, A. Roy, and N. Saxena, "Next generation 5G wireless networks: A comprehensive survey," *IEEE Commun. Surveys Tuts.*, vol. 18, no. 3, pp. 1617–1655, 3rd Quart., 2016.
[2] A. I. Sulyman, A. T. Nassar, M. K. Samimi, G. R. Maccartney, T. S. Rappaport, and A. Alsanie, "Radio propagation path loss models for 5G cellular networks in the 28 GHZ and 38 GHZ millimeter-wave bands," *IEEE Commun. Mag.*, vol. 52, no. 9, pp. 78–86, Sep. 2014.
[3] X. Wu and J.-J. Laurin, "Fan-beam millimeter-wave antenna design based on the cylindrical Luneberg lens," *IEEE Trans. Antennas Propag.*, vol. 55, no. 8, pp. 2147–2156, Aug. 2007.
[4] H.-T. Chou and Z.-D. Yan, "Parallel-plate Luneburg lens antenna for broadband multi-beam radiation at millimeter wave frequencies with design optimization," *IEEE Trans. Antennas Propag.*, vol. 66, no. 11, pp. 5794–5804, Nov. 2018.
[5] A. Rolland, R. Sauleau, and L. Le Coq, "Flat-shaped dielectric lens antenna for 60-GHz applications," *IEEE Trans. Antennas Propag.*, vol. 59, no. 11, pp. 4041–4048, Nov. 2011.
[6] N. T. Nguyen, R. Sauleau, and L. Le Coq, "Reduced-size double-shell lens antenna with flat-top radiation pattern for indoor communications at millimeter waves," *IEEE Trans. Antennas Propag.*, vol. 59, no. 6, pp. 2424–2429, Jun. 2011.
[7] A. Rolland, R. Sauleau, and M. Drissi, "Design of H-plane shaped flat lenses using a 2-D approach based on FDTD and genetic algorithm," in *Proc. Eur. Conf. Antennas Propag. (EuCAP)*, Apr. 2010, pp. 1–4.
[8] F. Scattone, M. Ettorre, R. Sauleau, N. T. Nguyen, and N. J. G. Fonseca, "Optimization procedure for planar leaky-wave antennas with flat-topped radiation patterns," *IEEE Trans. Antennas Propag.*, vol. 63, no. 12, pp. 5854–5859, Dec. 2015.
[9] Z.-Y. Zhang, Y. Li, G. Fu, S. Zuo, and N.-W. Liu, "Wideband circularly polarised array antenna with flat-top beam pattern," *IET Microw., Antennas Propag.*, vol. 9, no. 8, pp. 755–761, May 2015.
[10] U. A. Pawar, S. Chakraborty, T. Sarkar, A. Ghosh, L. L. K. Singh, and S. Chattopadhyay, "Quasi-planar composite microstrip antenna: Symmetrical flat-top radiation with high gain and low cross polarization," *IEEE Access*, vol. 7, pp. 68917–68929, 2019.
[11] A. Aghasi, H. Amindavar, E. L. Miller, and J. Rashed-Mohassel, "Flat-top footprint pattern synthesis through the design of arbitrary planar-shaped apertures," *IEEE Trans. Antennas Propag.*, vol. 58, no. 8, pp. 2539–2552, Aug. 2010.
[12] J. Sanford, "A Luneberg-lens update," *IEEE Antennas Propag. Mag.*, vol. 37, no. 1, pp. 76–79, Feb. 1995.
[13] L. C. Gunderson and G. T. Holmes, "Microwave Luneburg lens," *Appl. Opt.*, vol. 7, no. 5, pp. 801–804, May 1968.
[14] G. D. M. Peeler and H. P. Coleman, "Microwave stepped-index Luneburg lenses," *IRE Trans. Antennas Propag.*, vol. 6, no. 2, pp. 202–207, Apr. 1958.
[15] Z. Liu and P. Fan, "An effective handover scheme based on antenna selection in ground–train distributed antenna systems," *IEEE Trans. Veh. Technol.*, vol. 63, no. 7, pp. 3342–3350, Sep. 2014.
[16] C. Pfeiffer and A. Grbic, "A printed, broadband Luneburg lens antenna," *IEEE Trans. Antennas Propag.*, vol. 58, no. 9, pp. 3055–3059, Sep. 2010.
[17] L. Xue and V. F. Fusco, "Printed holey plate Luneburg lens," *Microw. Opt. Technol. Lett.*, vol. 50, no. 2, pp. 378–380, Dec. 2007.
[18] L. Xue and V. Fusco, "Patch-fed planar dielectric slab waveguide Luneburg lens," *IET Microw., Antennas Propag.*, vol. 2, no. 2, pp. 109–114, Mar. 2008.
[19] C. Hua, X. Wu, N. Yang, and W. Wu, "Air-filled parallel-plate cylindrical modified Luneberg lens antenna for multiple-beam scanning at millimeter-wave frequencies," *IEEE Trans. Microw. Theory Techn.*, vol. 61, no. 1, pp. 436–443, Jan. 2013.
[20] G. Godi, R. Sauleau, L. L. Coq, and D. Thouroude, "Design and optimization of three-dimensional integrated lens antennas with genetic algorithm," *IEEE Trans. Antennas Propag.*, vol. 55, no. 3, pp. 770–775, Mar. 2007.
[21] B. Fuchs, L. Le Coq, O. Lafond, S. Rondineau, and M. Himdi, "Design optimization of multishell Luneburg lenses," *IEEE Trans. Antennas Propag.*, vol. 55, no. 2, pp. 283–289, Feb. 2007.
[22] H. Mosallaei and Y. Rahmat-Samii, "Nonuniform Luneburg and two-shell lens antennas: Radiation characteristics and design optimization," *IEEE Trans. Antennas Propag.*, vol. 49, no. 1, pp. 60–69, Jan. 2001.
[23] B. Fuchs, R. Golubovic, A. K. Skrivervik, and J. R. Mosig, "Spherical lens antenna designs with particle swarm optimization," *Microw. Opt. Technol. Lett.*, vol. 52, no. 7, pp. 1655–1659, Jul. 2010.
[24] H.-T. Chou, Y.-S. Chang, H.-J. Huang, Z.-D. Yan, T. Lertwiriyaprapa, and D. Torrungrueng, "Optimization of three-dimensional multi-shell dielectric lens antennas to radiate multiple shaped beams for cellular radio coverage," *IEEE Access*, vol. 7, pp. 182974–182982, 2019.
[25] C. S. Silitonga, Y. Sugano, H. Sakura, M. Ohki, and S. Kozaki, "Optimum variation of the Luneberg lens for electromagnetic scattering calculations," *Int. J. Electron.*, vol. 84, no. 6, pp. 625–633, Jun. 1998.
[26] O. A. Abdul-Rahman, M. Munetomo, and K. Akama, "An adaptive parameter binary-real coded genetic algorithm for constraint optimization problems: Performance analysis and estimation of optimal control parameters," *Inf. Sci.*, vol. 233, pp. 54–86, Jun. 2013.

HSI-TSENG CHOU (Fellow, IEEE) received the B.S. degree in electrical engineering from National Taiwan University, in 1988, and the M.S. and Ph.D. degrees in electrical engineering from The Ohio State University (OSU), in 1993 and 1996, respectively.

He joined the ElectroScience Laboratory (ESL) with OSU, as a Graduate Research Associate, from 1991 to 1996. He was a Postdoctoral Researcher, from 1996 to 1998. He is currently a Distinguished Professor with the Department of Electrical Engineering, Graduate Institute of Communication Engineering, National Taiwan University, Taiwan. He has published more than 493 journal and conference papers. He holds over 40 patents. His research interests include wireless communication networks, antenna design, antenna measurement, electromagnetic scattering, asymptotic high-frequency techniques, such as uniform geometrical theory of diffraction (UTD), novel gaussian beam techniques, and UTD type solution for periodic structures.

Dr. Chou is a Fellow of IET and an Elected Member of URSI International Radio Science U.S. Commission B. He received many awards to recognize his distinguished contributions with the technological developments, such as the Distinguished Contribution Award in Promoting Inter-Academic and Industrial Cooperation with the Ministry of Education, the Distinguished Engineering Professor Award with the Chinese Institute of Engineers, and the Distinguished Electrical Engineering Professor Award with the Chinese Institute of Electrical Engineering. He received the University's Industrial Economics Contribution Award with the Ministry of Economics, in 2008, the National Industrial Innovation Awards-Key Technology Elite Award with the Ministry of Economics, in 2011, the Best Chapter Award, in 2012, the Industrial-Academia Collaboration Award with the Ministry of Economics, in 2017. He also received the outstanding branch counsellor awards with the IEEE, including the IEEE Headquarter R-10, Taipei Section, and the IEEE Technical Field Undergraduate Teaching Award, in 2014. He was elected as one of the nation's ten outstanding young persons with the Junior Chamber International, in 2004, a National Young Person Medal from the China Youth Corps, Taiwan, in 2005, and one of the top ten rising stars in Taiwan with the Central News Agency, Taiwan. He has served as the Chair for the IEEE AP-S Taipei Chapter. He serves the Chair for the EMC-S Taipei Chapter.

YI-SHENG CHANG was born in Yunlin, Taiwan, in 1980. He received the M.S. degree in communication engineering from Yuan Ze University, Taoyuan, Taiwan, in 2008, where he is currently pursuing the Ph.D. degree.

He held various positions as a Project Engineer and a Project Manager with the National Chung-Shan Institute of Science and Technology, Taoyuan, from 2002 to 2019, where he was involved with the design of radome, frequency selective surface (FSS), radar absorbing structure (RAS), and antennas. His current research interests include 3D FSS radome and lens antennas.

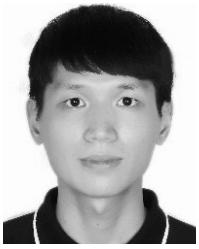

HAO-JU HUANG (Member, IEEE) was born in Taoyuan, Taiwan. He received the B.S. and M.S. degrees from Yuan Ze University, Taiwan, in 2016 and 2018, respectively. He is currently with the National Chung-Shan Institute of Technology, Taiwan. His research interests include simplified numerical techniques for fast design of phased array of antenna, compact range reflector design, low-frequency antenna design, and lens based beamforming networks. He received the Second Place Award with the Student Innovation Competition of the 2015 International Workshop on Electromagnetics, Applications and Student Innovation Competition. He was listed with the fifth place, Taiwan Creative Electromagnetic Implementation Competition (T-CEIC), in 2016.

ZHI-DA YAN (Student Member, IEEE) was born in Kaohsiung, Taiwan, in 1994. He received the B.S. degree in physics from the National University of Kaohsiung, Kaohsiung, in 2016. He is currently pursuing the Ph.D. degree with the Graduate Institute of Communication Engineering, National Taiwan University. His research interests include antenna design at millimetre-wave (mm-wave) frequencies for 5G applications and antenna measurements.

TITIPONG LERTWIRIYAPRAPA (Member, IEEE) received the B.S.Tech.Ed. degree in electrical engineering from the King Mongkut's University of Technology North Bangkok, in 1996, and the M.Eng. degree in electrical engineering from the King Mongkut's Institute of Technology Ladkrabang, in 2000, and the M.Sc. and Ph.D. degrees in electrical engineering from The Ohio State University, Columbus, OH, USA, in 2006 and 2007, respectively. He is currently an Associate Professor in electrical engineering with the Department of Teacher Training, King Mongkut's University of Technology North Bangkok. He holds a Board Committee of ECTI Association. He received the third place with the 2007 USNC/CNC URSI Student Paper Competition, Ottawa, Canada, and the Best Paper Award with the 2008 International Symposium on Antennas and Propagation (ISAP2008), Taiwan. His research interests include electromagnetic theory, metamaterial, asymptotic, computational electromagnetics, and hybrid methods.

DANAI TORRUNGRUENG (Senior Member, IEEE) received the B.Eng. degree in electrical engineering (EE) from Chulalongkorn University, Bangkok, Thailand, in 1993, and the M.S. and Ph.D. degrees in electrical engineering from The Ohio State University, in 1996 and 2000, respectively.

From 1995 to 2000, he was a Graduate Research Assistant (GRA) with the ElectroScience Laboratory, Department of Electrical Engineering, The Ohio State University. From 2002 to 2017, he was with the Electrical and Electronic Engineering Department, Faculty of Engineering and Technology, Asian University, Chonburi, Thailand. He is currently a Professor in electrical engineering with the Department of Teacher Training, Faculty of Technical Education, King Mongkut's University of Technology North Bangkok, Bangkok. He has authored *Meta-Smith Charts and Their Potential Applications* (Morgan and Claypool, 2010) and *Advanced Transmission-Line Modeling in Electromagnetics* (Charansanitwong Printing, 2012). From 2004 to 2009, he invented generalized Smith charts, called T-charts or Meta-Smith charts, for solving several problems associated with conjugately characteristic-impedance transmission lines (CCITLs) and bi-characteristic-impedance transmission lines (BCITLs), including their useful applications in applied electromagnetics. His research interests include electromagnetic sensors, fast computational electromagnetics, rough surface scattering, propagation modeling, electromagnetic wave theory, microwave theory and techniques, and antennas. He is a member of ECTI. He is also a Co-Founder with the Innovative Electromagnetics Academy of Thailand (iEMAT), in 2013. In 2000, he received the Award with the National URSI Student Paper Competition, National Radio Science Meeting, Boulder, Colorado, in 2000. He served as an ECTI Technical Chair in Electromagnetics, from 2014 to 2017. He also served as a TPC Co-Chair for TJMW2016, a Vice Co-Chair for TJMW2017, and the TPC Chair for ISAP2017.